

High-resolution fiber optic temperature sensors using nonlinear spectral curve fitting technique

Z. H. Su, J. Gan, Q. K. Yu, Q. H. Zhang, Z. H. Liu et al.

Citation: *Rev. Sci. Instrum.* **84**, 045002 (2013); doi: 10.1063/1.4802684

View online: <http://dx.doi.org/10.1063/1.4802684>

View Table of Contents: <http://rsi.aip.org/resource/1/RSINAK/v84/i4>

Published by the [American Institute of Physics](http://www.aip.org).

Additional information on *Rev. Sci. Instrum.*

Journal Homepage: <http://rsi.aip.org>

Journal Information: http://rsi.aip.org/about/about_the_journal

Top downloads: http://rsi.aip.org/features/most_downloaded

Information for Authors: <http://rsi.aip.org/authors>

ADVERTISEMENT

physicstoday

Comment on any
Physics Today article.

Measured energy in Japan
David von Seggern
(dvseg@seismo.unr.edu) University of Nevada
July 2012, page 10
DIGITAL OBJECT IDENTIFIER
<http://dx.doi.org/10.1063/PT.3.1619>

Comment on this article
By the act of hitting a ball with a bat, one calculates the force energy to deliver the ball to its new location, but one must also take into account that the ball extended its energy to the struck team, which became struck by the ball as its momentum ceased and passed energy to the struck team. Therefore the parameters of the damage extend into the future when the received energy to that pushed upon, later becomes released in a new event. Perhaps calculations of one added that in, while another's calculations did not. E.M.C.
Written by Edgar McCarvill, 14 July 2012 19:59

High-resolution fiber optic temperature sensors using nonlinear spectral curve fitting technique

Z. H. Su,¹ J. Gan,^{2,a)} Q. K. Yu,³ Q. H. Zhang,¹ Z. H. Liu,³ and J. M. Bao^{1,a)}

¹Department of Electrical and Computer Engineering, University of Houston, Houston, Texas 77204, USA

²Idaho National Laboratory, Nuclear Fuels and Materials Division, Idaho Falls, Idaho 83415, USA

³Ingram School of Engineering and Materials Science, Engineering and Commercialization, Texas State University, San Marcos, Texas 78666, USA

(Received 12 January 2013; accepted 8 April 2013; published online 29 April 2013)

A generic new data processing method is developed to accurately calculate the absolute optical path difference of a low-finesse Fabry-Perot cavity from its broadband interference fringes. The method combines Fast Fourier Transformation with nonlinear curve fitting of the entire spectrum. Modular functions of LabVIEW are employed for fast implementation of the data processing algorithm. The advantages of this technique are demonstrated through high performance fiber optic temperature sensors consisting of an infrared superluminescent diode and an infrared spectrometer. A high resolution of 0.01 °C is achieved over a large dynamic range from room temperature to 800 °C, limited only by the silica fiber used for the sensor. © 2013 AIP Publishing LLC. [<http://dx.doi.org/10.1063/1.4802684>]

I. INTRODUCTION

Fiber-based low-finesse Fabry-Perot (F-P) cavities are core components of a variety of sensors.¹⁻⁵ Using suitable configurations, quantities such as temperature,^{1-3,5} pressure,^{5,6} strain,^{2,4} and micro-displacement⁷ can be obtained from the gap distance or optical path difference (OPD) of the cavity. As such, a precise OPD determination is essential to the performance of these sensors. Among various optical techniques used to extract OPD, dispersive white-light interferometry based on a broadband light source and a dispersive spectrometer shows advantages over other techniques.^{2,4,8-16} Not only is this due to the interference fringes that contain sufficient spectral information for us to calculate OPD, but the technique involves no moving mechanical parts as well. However, previously reported data processing techniques only make use of partial information of the interference spectrum by tracking the positions of one or two interference fringes.^{2,4,9,10,12} Because these wavelength tracking techniques still depend on the positions of one or two interference fringes, their resolutions can be further improved if more information from the interference fringes can be utilized. Fast Fourier Transformation (FFT) is a technique that uses the entire interference spectrum to directly calculate the OPD;¹³⁻¹⁶ however, it also introduces a larger OPD uncertainty than peak tracking methods because of the uncertainty in determining FFT peaks. An OPD resolution of ± 50 nm was reported.¹⁵ A higher resolution of 3 nm was achieved by combining FFT with additional data analysis involving inverse FFT, phase unwrapping, and linear regression.^{13,16} Here, we present a generic data processing method to precisely calculate the OPD by fitting the entire interference fringes. To demonstrate this new technique, we fabricated several fiber optical temperature sensors. We then used LabVIEW modu-

lar functions to implement the algorithm so that the technique can be readily adopted by the optical sensing community.

II. SENSOR DESIGN AND FABRICATION

Figure 1 shows the schematic of a fiber optic temperature sensor based on a low finesse F-P cavity and the associated white-light interferometry. The system consists of a sensor head, an infrared light source, an infrared array detector, and a 2×1 50/50 fiber coupler, which couples light from the infrared source to the sensor head and then back to the detector. LabVIEW is used to communicate with the detector and perform data acquisition and processing. The coupler (Thorlabs FC1310-70-50-APC) is a single mode fiber operating at telecommunication wavelength of 1310 nm. A superluminescent diode (SLD) with the same operating wavelength was also selected as an infrared light source. The SLD produces up to 12.5 mW light with 80 nm bandwidth for white light interferometry. An OceanOptics near-infrared InGaAs array detector (NIRQUEST 512) was used for fast spectral acquisition with high sensitivity. SLDs centered at 850 nm were previously used by many groups.^{2,4,9,12} We choose a 1320-nm SLD because (1) its telecommunication wavelength enables remote sensing and (2) interference fringes can be better resolved due to a larger optical dispersion of the grating at longer wavelengths.

The sensor head is a low-finesse F-P cavity made of two facets of the single mode silica fibers confined in an alumina tube. The fibers are bonded to the tube at both ends with a distance of 4–5 mm. We set initial room temperature cavity length between 50 and 100 μm so that enough fringes will be obtained for an accurate cavity length determination. The cavity length increases as temperature increases because of a much larger thermal expansion coefficient of alumina than silica; this forms the basis for the temperature sensing of the cavity. One advantage of such a fiber-based F-P cavity is its

^{a)}Authors to whom correspondence should be addressed. Electronic addresses: Jian.Gan@inl.gov and jbao@uh.edu

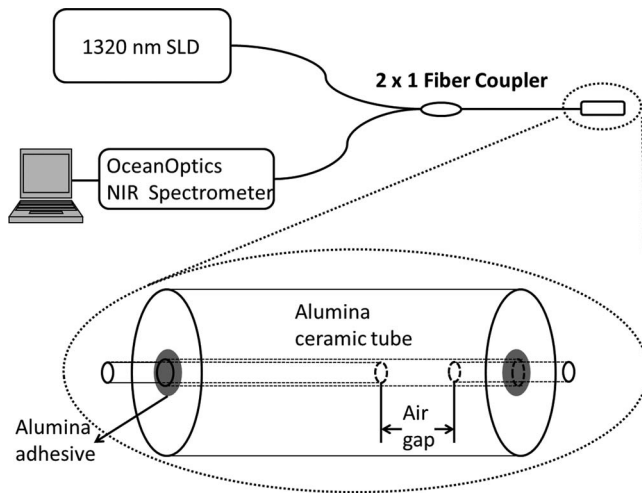


FIG. 1. Schematic of a fiber optic temperature sensor.

relative simplicity in fabrication: two facets are created by a fiber cleaver without mechanical polishing; no optical alignment is needed for two facets of the cavity because of the alumina tube.

III. DATA PROCESSING AND ANALYSIS

Figure 2(a) shows typical interference spectra from two sensors with different initial cavity lengths at room temperature. Both spectra exhibit a much higher interference visibility than those previously reported.^{10,17} The envelope of spectra represents the spectrum of SLD (bottom curve of

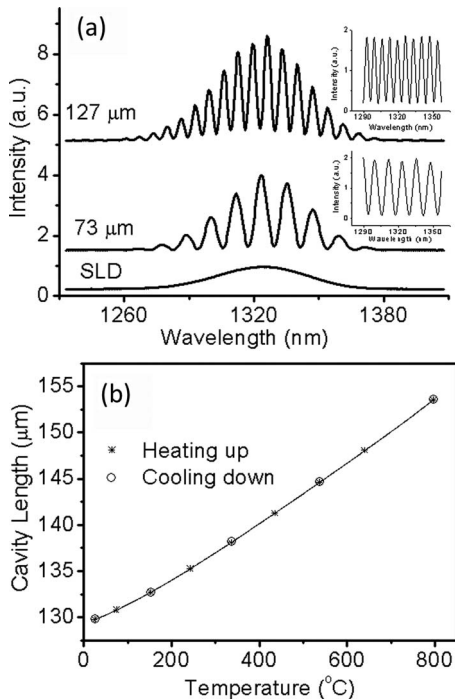


FIG. 2. (a) Spectrum of the SLD at a low current (bottom) and interference fringes from the two sensors at room temperature. Spectra are shifted vertically for clarity. Insets are the corresponding interference fringes normalized by the spectrum of SLD. (b) Cavity length as a function of temperature during heating and cooling. The solid line is a polynomial fit.

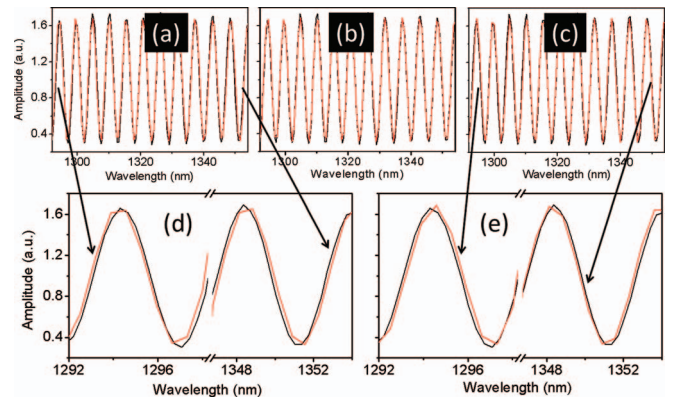


FIG. 3. Nonlinear curve fitting using Eq. (1). Data are in black and fittings are in red. (a)–(c) Fits with three different cavity lengths L . (b) gives the best fit of 161475.18 nm, (a) and (c) give shorter (160813.80 nm) and longer (162136.62 nm) L by ~ 660 nm, respectively. (d) and (e) are close-up views of curves at shorter and longer wavelength sides of (a) and (c), respectively.

Fig. 2(a)), which is obtained using LabVIEW's low-pass filtering of the interference fringes. By normalizing the interference fringes with the spectrum of SLD, sinusoidal interference fringes with near-uniform amplitude are obtained (insets of Fig. 2(a)). As discussed in detail below, the cavity length can be precisely obtained from such sinusoidal interference fringes using nonlinear curve fitting. Figure 2(b) shows the evolution of cavity length during heating and cooling. No noticeable hysteresis is observed, indicating that the cavity can be very well suited for temperature sensing. The curve in Fig. 2(b) also provides calibration for the sensor, indicating an average sensitivity of $30 \text{ nm}/^\circ\text{C}$.

The normalized spectra in the insets of Fig. 2(a) can be described as^{10,12}

$$I(\lambda) = A + \gamma * \cos\left(\frac{4\pi L}{\lambda} + \pi\right), \quad (1)$$

where A and γ are constants, π is due to the phase shift of the reflected beam from the air/silica interface, and L is the cavity length. In principle, using nonlinear curve fitting—a standard function in commercial data processing software such as LabVIEW or Origin—the length L can be uniquely and quickly determined. However, as we show below, initial fitting parameters are important to obtain the best fitting for the periodic function of Eq. (1).

If Eq. (1) is used to fit the data with the initial L confined in a wide range (i.e., $20 \mu\text{m} < L < 180 \mu\text{m}$), then three different lengths will typically be obtained, and the result from the fitting program will randomly fluctuate among these three values. Fitting curves from the three lengths as provided in this example are shown in Figs. 3(a)–3(c). As can be seen, all three fits represent the data quite well, and are regarded as the best fit by the fitting program. But close-up views shown in Figs. 3(d) and 3(e) reveal that the fits in Figs. 3(a) and 3(c) deviate from the original curves at short and long wavelengths. Specifically, the fit in Fig. 3(d) shows a phase advance near 1294 nm, but a phase delay near 1352 nm. In the central region near 1320 nm, the fit overlaps with the data very well. The length from this fitting is shorter than the best fitting value L_0 in Fig. 3(b) by $\lambda/2 \sim 660$ nm. According to Eq. (1), this

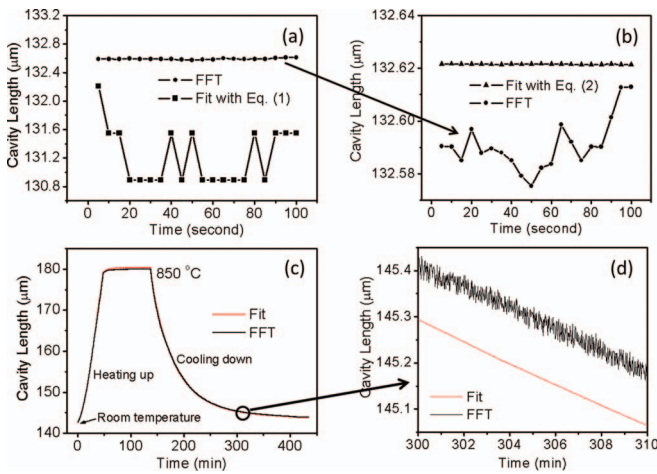


FIG. 4. Evolution of cavity length calculated using three different methods: (1) direct nonlinear fit using λ as a variable, (2) FFT, and (3) nonlinear fit using $1/\lambda$ as a variable. (a) Cavity lengths at room temperature calculated using methods 1 (square) and 2 (dot). Note that data for FFT and nonlinear fit were taken at different times so that their cavity lengths do not overlap. (b) Room temperature cavity lengths calculated using method 3 (triangle). The FFT result is the same as in (a), but the vertical scale is 40 times smaller. Same data for FFT and fit. (c) Evolution of cavity length during heating and cooling monitored using methods 2 and 3. (d) Close-up view of cavity length evolution near 300 min.

difference in cavity length creates a phase shift of 2π near the center wavelength of 1320 nm so that the fitting at 1320 nm is not affected. The fit in Fig. 3(e) exhibits an opposite behavior with a longer cavity length by 660 nm.

The problem with nonlinear curve fittings using Eq. (1) without good initial parameters can be clearly seen in Figure 4(a), where the cavity length was monitored over a short period of time at room temperature. Based on this sensitivity, the fluctuation of temperature is found to be $\sim 20^\circ$. In order to obtain the initial value of L for the fitting, we introduced $k = 1/\lambda$ as a new variable, and converted Eq. (1) to Eq. (2), as follows:

$$I(\lambda) = A + \gamma \cos(4\pi kL + \pi). \quad (2)$$

We can then use FFT to obtain a very good estimate of L from Eq. (2). It should be noted that the initial spectra, as shown in Figs. 2 and 3, use λ as a variable so the data points are evenly spaced in λ . The change of variable from wavelength λ to wave number k makes the result from Eq. (2) not evenly spaced in k . In order to use FFT and then use nonlinear curve fitting to extract L from Eq. (2), we interpolate spectrum by using “resample” of LabVIEW. Figure 4(b) shows a much stable cavity length after using L from FFT to fit Eq. (2). The fluctuation is reduced to 0.2 nm, corresponding to a temperature resolution of 0.01°C . As a comparison, we also plotted the cavity length obtained using FFT of the resampled Eq. (2). As can be seen in Figs. 4(a) and 4(b), the FFT cavity length suffers less fluctuation as compared with the initial curve fitting using Eq. (1), but is still as large as 10s nm. Note that the FFT cavity length is plotted in both Figs. 4(a) and 4(b), but the scale in Fig. 4(b) is 40 times smaller than the scale in Fig. 4(a).

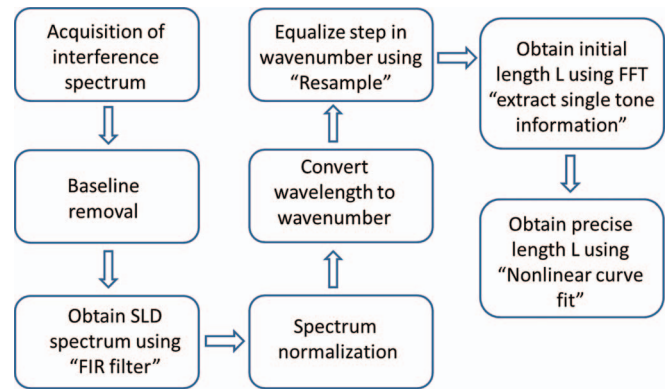


FIG. 5. Flow chart used to calculate the absolute cavity length using revised nonlinear curve fitting and LabVIEW internal functions.

Figures 4(c) and 4(d) show the evolution of the cavity length obtained using FFT and the subsequent curve fitting of Eq. (2) using FFT length as an initial parameter. A clear improvement in temperature resolution can be seen. The length fluctuation from FFT is ~ 20 nm, corresponding to $1^\circ\text{--}2^\circ$. Similar FFT fluctuation was reported before.¹⁵ It was also found that results from FFT may not overlap with the result from the curve fitting. This is because the L from FFT is based on the position of FFT spectrum with the highest intensity, which can be quite different from the position obtained by fitting the FFT peak.

Figure 5 shows the flow chart of our curve fitting technique to obtain the absolute cavity length. This technique makes use of existing functions provided by LabVIEW so that software development time can be reduced. The speed of processing is mainly limited by the spectrum acquisition time, typically 100 ms. In some cases, the cavity length shows jumping as shown in Figure 4(a) due to a large fluctuation of cavity length from FFT. This jumping can be eliminated when the last cavity length is used as an initial parameter for the fitting. Such strategy was employed to monitor the temperature evolution in Fig. 4(c). In addition to its high accuracy and sensitivity, this technique has other benefits as compared with the wavelength tracking method. For example, the temperature can be obtained at any time without utilizing prior spectral information, such as fringe order. The temperature will also not be affected by the power fluctuation of SLD. In the event of a measurement interruption, the initial recovered temperature reading by the FFT method will be within $1\text{--}2^\circ\text{C}$ of the actual temperature.

It was proposed that there is an additional cavity length dependent phase in Eq. (1) due to the coupling between incident and reflected light.^{17,18} Such a phase has not been taken into consideration in wavelength tracking methods because it is difficult to measure. This phase is important for the basic understanding of interference fringes, but the effect of such a phase on this curve fitting method and the accuracy of the temperature is negligible based on the following reasons: First, the temperature from the sensor will be calibrated according to the curve in Fig. 2(b). As long as there is a one-to-one relationship between cavity length and temperature, the obtained temperature is always accurate. Second, as shown in

Ref. 17, the change of the phase becomes so small at large cavity lengths; it can be neglected in our cases. Third, because this phase originates from the increased OPD than the absolute cavity difference due to beam divergence, this phase change can be described by introducing an effective cavity length L_{eff} . In other words, the L obtained from curve fitting can be the effective optical path length that is slightly larger than the real cavity length. As discussed above, whether it is a real cavity length with a negligible phase change or an effective cavity length will not affect the reading of the cavity temperature.

In summary, we developed and demonstrated a new data processing technique to precisely extract absolute cavity length of a F-P sensor; we subsequently demonstrate fiber optic temperature sensors with temperature resolution as high as 0.01 °C. Such a technique provides a higher resolution over a wide dynamic range. By taking advantage of new commercial software and hardware, such as LabVIEW, infrared SLD, high performance portable spectrometer, and computer, this new data processing technique provides faster, accurate, and more reliable readings of many sensors based on the Fabry-Perot cavity.

ACKNOWLEDGMENTS

This work is supported through the INL Laboratory Directed Research and Development (LDRD) Program under (U.S.) Department of Energy (DOE) Idaho Operations Office Contract No. DE-AC07-05ID14517. Partial support from the Welch Foundation (E-1728) is acknowledged. This submitted article was authored by a contractor of the U.S.

Government under DOE Contract No. DE-AC07-05ID14517. Accordingly, the U.S. Government retains and the publisher, by accepting the article for publication, acknowledges that the U.S. Government retains a nonexclusive, paid-up, irrevocable, worldwide license to publish or reproduce the published form of this article, or allow others to do so, for U.S. Government purposes.

- ¹H. S. Choi, H. F. Taylor, and C. E. Lee, *Opt. Lett.* **22**, 1814 (1997).
- ²T. Liu, G. F. Fernando, Z. Y. Zhang, and K. T. V. Grattan, *Sens. Actuators A* **80**, 208 (2000).
- ³A. Wang, S. Gollapudi, R. G. May, K. A. Murphy, and R. O. Claus, *Smart Mater. Struct.* **4**, 147 (1995).
- ⁴V. R. Machavaram, R. A. Badcock, and G. F. Fernando, *Sens. Actuators, A* **138**, 248 (2007).
- ⁵A. Wang, H. Xiao, J. Wang, Z. Y. Wang, W. Zhao, and R. G. May, *J. Lightwave Technol.* **19**, 1495 (2001).
- ⁶H. Xiao, J. D. Deng, Z. Y. Wang, W. Huo, P. Zhang, M. Luo, G. R. Pickrell, R. G. May, and A. B. Wang, *Opt. Eng.* **44**, 054403 (2005).
- ⁷T. C. Li, R. G. May, A. Wang, and R. O. Claus, *Appl. Opt.* **36**, 8858 (1997).
- ⁸U. Schnell, R. Dandliker, and S. Gray, *Opt. Lett.* **21**, 528 (1996).
- ⁹S. A. Egorov, A. N. Mamaev, and A. S. Polyantsev, *J. Lightwave Technol.* **13**, 1231 (1995).
- ¹⁰B. Qi, G. R. Pickrell, J. C. Xu, P. Zhang, Y. H. Duan, W. Peng, Z. Y. Huang, W. Huo, H. Xiao, R. G. May, and A. Wang, *Opt. Eng.* **42**, 3165 (2003).
- ¹¹Y. J. Rao and D. A. Jackson, *Meas. Sci. Technol.* **7**, 981 (1996).
- ¹²J. Tapia-Mercado, A. V. Khomenko, and A. Garcia-Weidner, *J. Lightwave Technol.* **19**, 70 (2001).
- ¹³F. B. Shen and A. B. Wang, *Appl. Opt.* **44**, 5206 (2005).
- ¹⁴A. Majumdar and H. Huang, *Appl. Opt.* **47**, 2821 (2008).
- ¹⁵C. Boulet, M. Hathaway, and D. A. Jackson, *Opt. Lett.* **29**, 1602 (2004).
- ¹⁶J. Wang, B. Dong, E. Lally, J. Gong, M. Han, and A. B. Wang, *Opt. Lett.* **35**, 619 (2010).
- ¹⁷C. Ma, B. Dong, J. M. Gong, and A. B. Wang, *Opt. Express* **19**, 23727 (2011).
- ¹⁸M. Han, Y. Zhang, F. B. Shen, G. R. Pickrell, and A. B. Wang, *Opt. Lett.* **29**, 1736 (2004).